# Ring Artifact Reduction in Sinogram Space Using Deep Learning

*M. Nauwynck**, *S. Bazrafkan**, *A. H. van Heteren*†‡§ , *J. De Beenhouwer**, *J. Sijbers**

* imec-Vision Lab, Department of Physics, University of Antwerp, Belgium
† Sektion Mammalogie, Zoologische Staatssammlung München, Staatliche Naturwissenschaftliche Sammlungen Bayerns, Munich, Germany ‡ GeoBio-Center, Ludwig-Maximilians-Universität München, Munich, Germany
§ Department Biologie II, Ludwig-Maximilians-Universität München, Munich, Germany

***Abstract*—Ring artifacts are a type of reconstruction artifact that is common in X-Ray CT. Recently, methods based on deep learning have been proposed to reduce ring artifacts in reconstructed images. These methods are dependent on the choice of reconstruction algorithm and often rely on a polar coordinate transformation. Methods that directly operate in sinogram space do not feature this dependency, do not require a coordinate transformation while also operating in the space where ring artifacts originate.**

**In this paper, we propose a deep neural network with a custom loss function that operates exclusively in sinogram space for ring artifact reduction. Results on real and simulated data show that our method has similar or better performance compared to other ring artifact reduction techniques that also operate exclusively in sinogram space.**

***Index Terms*—Deep learning, Tomography, Ring Artifact**

## I. Introduction

RING artifacts are a type of reconstruction artifact that is common in X-ray CT. They appear as a series of lines that overlay the sinogram. Ring artifacts typically originate from the X-ray hardware. In a synchrotron, for instance, the X-ray detector, source and/or the monochromator may cause ring artifacts [1, 2] due to variations in detector element sensitivity [3, 4], defective elements [5], changes in sensitivity between flatfield corrections [4], insufficient flatfield correction [5], variable (non-linear) response to beam hardening [4–6], dusty or damaged scintillator screens [5, 7], varying scintillator thickness [2, 4, 8], imperfections in the optical coupling system [2] and drift or mechanical vibrations of a monochromator [2]. After tomographic reconstruction, these deviations appear as (partial) concentric circles [4] (see Fig. 1). As these rings have an adverse effect on further image analysis, it is desirable to reduce them.

Common methods that attempt to reduce ring artifacts can be categorized in three groups: methods that operate in sinogram space (e.g. [1–3, 5, 7, 8]), image space (e.g. [3, 4, 9]) or both spaces (e.g. [10–12]).

Recently, deep learning methods have been proposed to reduce ring artifacts in CT images [11–13]. Wang, Li, and Enoh [11] use a generative adversarial network with adversarial loss, perceptual loss and a unidirectional relative total variation loss. Reconstructed images are first transformed from cartesian to polar coordinates as a preprocessing step. The

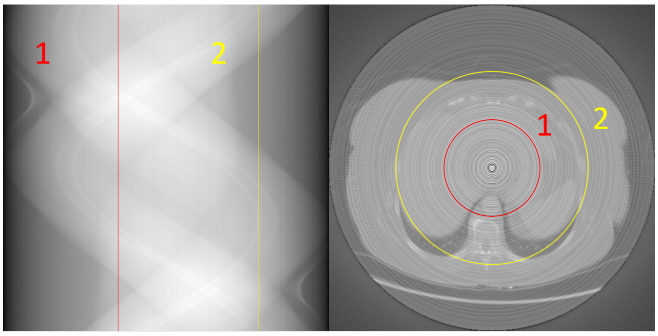


Figure 1: Artifacts on sinogram and reconstructed image.

method by Chao and Kim [9] also operates in image space with use of polar coordinates. Ring artifacts are first detected by using a smoothing operation, after which a trained radial basis function neural network is applied to reduce the artifacts on a pixel-basis. Finally, Fang, Li, and Chen [12] combined both spaces in their work to estimate an artifact map, which is subsequently subtracted from the initial reconstruction.

Multiple disadvantages are encountered when using methods that operate exclusively in image space. One is the need for correctly selecting the center for the coordinate transformation. A second limitation arises when working with reconstructed images of low quality. Few-view or limited angle CT are examples where the reconstructed image quality is significantly degraded and the artifacts have a less distinct pattern. A final limitation when working exclusively in image space relates to the fact that ring artifacts originate in sinogram space. They can be viewed as signals that are local, i.e. at some detector channel. After tomographic reconstruction, this locality is lost. Finally, the appearance of ring artifacts in image space depends on the tomographic reconstruction method that was applied to obtain the image. This dependency implies that separate deep neural networks need to be trained for different reconstruction algorithms as the reconstruction of a sinogram with the same line artifact may vary significantly depending on the choice of algorithm.

To avoid the above mentioned, a deep learning approach is proposed that works exclusively in sinogram space. To the best of our knowledge, deep learning has not yet been applied to sinogram preprocessing for ring artifact reduction. The

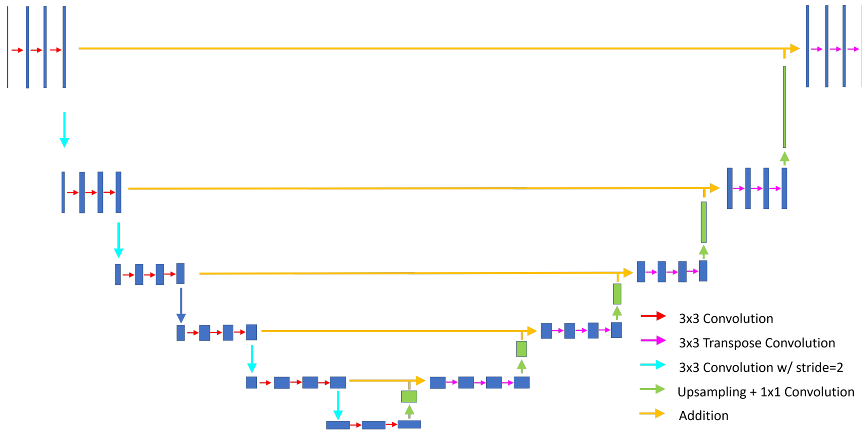


Figure 2: Network architecture

proposed method is independent of the choice of reconstruction algorithm, does not rely on a coordinate transformation and operates in the space where the artifact originates. To achieve this, a deep neural network, similar to U-Net [14], is implemented and trained on simulated data. Results on both simulated and real data are compared to other methods that operate in sinogram space. Our findings support the relevance of exclusively using sinograms in ring artifact reduction.

## II. Methodology

Similar to other papers that operate in sinogram space to reduce metal artifacts [15, 16], a deep neural network was implemented that is based on a U-Net architecture [14]. A deep neural network (DNN) is a model that consists of several processing units also known as layers. These layers could be convolution/deconvolution, pooling/unpooling, and dense operations. In the current study, a DNN similar to U-Net was implemented (Fig. 2) to process sinogram data as to reduce ring artifacts. It is a fully convolutional DNN with a downsampling operation after every three convolutional layers. Downsampling is accomplished by using a 3×3 convolutional operation with a stride equal to 2. Note that the number of channels is doubled after each downsampling operation in order to preserve the information flow throughout the network. The second half of the network consists of deconvolution and upsampling layers to recover the signal back to the input size. Note that every upsampling operation is followed by a 1×1 convolutional layer. There are several skip connections inside the network architecture indicated by yellow arrows in Fig. 2. The skip connections are not used in the original implementation and make the model more parameter-efficient. The skip connections transfer the high-frequency bands from the early stages into the deeper layers which plays an important role in preserving the sharpness of the output. The ReLU activation function [17] is applied after each convolution, except for the last layer which has no activation function.

The parameters were optimized using a combined loss function. The first component, $l_1$, is a normalized L1 loss between the network output and the target tensor, defined by Eq. (1), with $N$ the number of samples and $y$ and $\hat{y}$ the expected and predicted result, respectively.

$$l_1 = \frac{\sum_{n=1}^{N} |y_n - \hat{y}_n|}{\sum_{n=1}^{N} |y_n|} \tag{1}$$

The second loss, $l_2$, is given by Eq. (2) wherein a normalized L1 loss is computed after convolving the difference between the predicted and expected result with the vertical kernel, $w$, of the Sobel operator.

$$l_2 = \frac{\sum_{n=1}^{N} \big|w * (y_n - \hat{y}_n)\big|}{\sum_{n=1}^{N} |w * y_n|} \tag{2}$$

The final loss function, $l$, is the weighted summation of the two separate components as shown in Eq. (3).

$$l = \alpha l_1 + \beta l_2 \tag{3}$$

Normalizing the loss functions allows to easily set and understand their relative contribution. Our results were acquired with weights $\alpha$ and $\beta$ set to 0.8 and 0.2, respectively. These values were selected through experimentation.

The Adam optimizer [18] was utilized in the training procedure with an initial learning rate equal to $3 \times 10^{-3}$ and other hyperparameters left to their default values. A dynamic learning rate was used during training, reducing the learning rate by 10% if the loss on training data had not decreased in the 5 previous epochs. The model was built in Python version 3.6 using Tensorflow version 2.0 [19] as the framework of choice and was trained for 180 epochs on a NVIDIA Tesla K80 GPU using a batch size of 128.

## III. Experiments

### A. Dataset

In order to provide the training database, ring artifacts were simulated on clean images. To this extent, images from the The Cancer Imaging Archive [20] were used (45640 medical images, resized to 256 by 256 pixels). Every image, no matter the modality, was included in the dataset. This ensured that the network observed a large variation of sinograms during training. Fig. 1 shows an example of a sinogram with simulated ring artifacts and the reconstructed image.

Sinograms were simulated in a parallel beam set-up through use of the ASTRA Toolbox [21] and line artifacts were added onto them. To accurately model statistical parameters of the artifact magnitude, the available datasets from Tomobank [22] with ring artifacts were analyzed. A smoothing method, part of the Tomopy toolbox [23], was applied to an image as to strongly reduce ring artifacts. By comparing the smoothed and original image, a normal distribution for the mean artifact magnitudes was estimated. Corresponding variances were estimated as well. To generate artifacts, a mean artifact magnitude value was randomly sampled from the estimated distribution for every detector channel. Variances for each mean artifact magnitude were computed, resulting in normal distributions for every affected detector channel. The resulting normal distributions were randomly sampled to generate ring artifacts for all projection angles. Finally, the artifacts were added onto the artifact-free sinogram. The dataset was split in a training, validation and test set with 42240, 1000 and 2400 samples, respectively.

### B. *Evaluation*

The performance of our method in terms of peak signal-to-noise ratio (PSNR) and structured similarity (SSIM) [24] was compared to that of four other methods that operate in sinogram space: wavelet-Fourier filtering (FW) [25], the generalized Titarenko's algorithm (TI) [26], a based filtering approach (BF) [1] and a smoothing filtering. Out of all the available methods in the Tomopy library, these four were selected based on their better performance on real samples with ring artifacts.

Ring artifacts in 2400 simulated sinograms were suppressed using our approach and the four reference methods. These samples were not seen by the neural network during training. The simulation principle, however, was the same as for the training samples. In all evaluations, filtered backprojection was used as the reconstruction technique. PSNR and SSIM were subsequently computed for the reconstructed images.

To assess the effect of the proposed method on real data, it was tested on real sinograms of a bone sample, alongside with the reference methods. The sample was acquired with TESCAN XRE's UniTOM XL scanner using a cone beam set-up.

## IV. Results

### A. *Simulated data*

Fig. 3a shows PSNR values for the different ring artifact reduction algorithms. Our method has a median PSNR that is at least 2dB higher than the reference methods. These results show that our method is able to reduce ring artifacts to a larger extent relative to the other methods. The variation seen in the results is small compared to other methods, with the exception of the generalized Titarenko's algorithm. These results indicate that our method performs well on sinograms that belong to a variety of images (differing in contrast and brightness values for instance).

Similar observations can be made when considering the SSIM values (Fig. 3b). In general, the best results are still achieved with a deep learning approach. The SF, FW and BF approach show a larger variance, while also having a lower median. The generalized Titarenko's approach shows a similar range of scores like the other methods when using SSIM as metric.

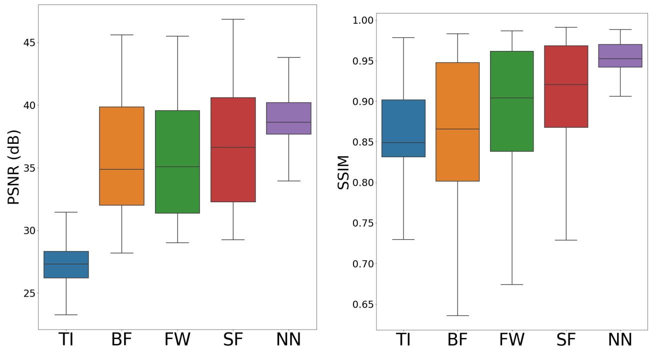


(a) (b)

Figure 3: PSNR (a) and SSIM (b) values for different ring artifact reduction techniques.

### B. *Real data*

Fig. 4 illustrates the results of all methods on real data. In this case, only a visual comparison can be made, as no ground truth is available. All methods are able to reduce ring artifacts to a comparable degree. The thin ring artifacts are largely reduced in all cases. However, there are still some (newly introduced) artifacts present. Most notable is the remaining presence of the thicker ring artifacts for all methods. These types of artifacts are not included in the simulation data and are consequently not reduced by the neural network.

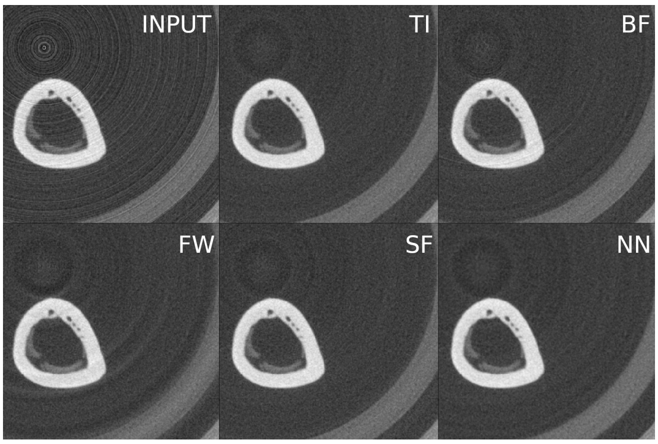


Figure 4: The unprocessed reconstruction (INPUT) as well as five different ring artifact reduction techniques applied to a reconstruction of a real sample with ring artifacts.

.

## V. Discussion

In this paper, a U-Net-like deep neural network for sinogram preprocessing was proposed to prevent ring artifacts in the reconstructed image. On a simulated dataset of 2400 samples, unseen by the neural network, significantly higher PSNR and SSIM values were reached compared to four reference methods. These results indicate that our method was able to reduce ring artifacts to a larger degree.

Due to the lack of a dataset consisting of the same sinograms with and without ring artifacts, data was simulated in this work. Nevertheless, visual assessment of ring artifact reduction on a real sample showed results comparable to other methods that operate in sinogram space. This is an indication that our method is able to generalize beyond simulated data and can also be applied to real data. However, despite our best attempts to accurately model ring artifacts, they inevitably differ from real world samples. The presence of thicker rings in Fig. 4 illustrates this problem. Consequently, caution has to be taken when making interpretations on performance for real data, based on the results for simulated data.

In future work, ring artifact reduction methods operating in image space will be included in the study. Ring artifacts will also be simulated more realistically, for instance by including thicker bands. This will allow us to see whether or not ring artifacts can be reduced to a larger degree.

## Acknowledgment

This research received funding from the Flemish Government under the "Onderzoeksprogramma Artificiële Intelligentie (AI) Vlaanderen" programme as well as from the Research Foundation Flanders (FWO) through the MetroFlex project S004217N. Real data was acquired with TESCAN XRE's UniTOM XL scanner.

## References

[1] N. T. Vo, R. C. Atwood, and M. Drakopoulos, "Superior techniques for eliminating ring artifacts in X-ray microtomography", *Optics Express*, vol. 26, no. 22, p. 28 396, Oct. 2018.

[2] L. C. P. Croton, G. Ruben, K. S. Morgan, *et al.*, "Ring artifact suppression in X-ray computed tomography using a simple, pixel-wise response correction", *Optics Express*, vol. 27, no. 10, p. 14 231, May 2019.

[3] R. A. Ketcham, "New algorithms for ring artifact removal", in *Developments in X-Ray Tomography V*, U. Bonse, Ed., SPIE, Aug. 2006.

[4] J. Sijbers and A. Postnov, "Reduction of ring artefacts in high resolution micro-CT reconstructions", *Physics in Medicine and Biology*, vol. 49, no. 14, N247–N253, Jul. 2004.

[5] E. M. A. Anas, S. Y. Lee, and M. K. Hasan, "Removal of ring artifacts in CT imaging through detection and correction of stripes in the sinogram", *Physics in Medicine and Biology*, vol. 55, no. 22, pp. 6911–6930, Nov. 2010.

[6] F. Vidal, J. Létang, G. Peix, *et al.*, "Investigation of artefact sources in synchrotron microtomography via virtual X-ray imaging", *Nuclear Instruments and Methods in Physics Research Section B: Beam Interactions with Materials and Atoms*, vol. 234, no. 3, pp. 333–348, Jun. 2005.

[7] S. Rashid, S. Y. Lee, and M. K. Hasan, "An improved method for the removal of ring artifacts in high resolution CT imaging", *EURASIP Journal on Advances in Signal Processing*, vol. 2012, no. 1, Apr. 2012.

[8] W. Vågberg, J. C. Larsson, and H. M. Hertz, "Removal of ring artifacts in microtomography by characterization of scintillator variations", *Optics Express*, vol. 25, no. 19, p. 23 191, Sep. 2017.

[9] Z. Chao and H.-J. Kim, "Removal of computed tomography ring artifacts via radial basis function artificial neural networks", *Physics in Medicine & Biology*, vol. 64, no. 23, p. 235 015, 2019.

[10] M. Salehjahromi, Q. Wang, Y. Zhang, *et al.*, "A new iterative algorithm for ring artifact reduction in CT using ring total variation", *Medical Physics*, vol. 46, no. 11, pp. 4803–4815, Sep. 2019.

[11] Z. Wang, J. Li, and M. Enoh, "Removing ring artifacts in CBCT images via generative adversarial networks with unidirectional relative total variation loss", *Neural Computing and Applications*, vol. 31, no. 9, pp. 5147–5158, Jan. 2019.

[12] W. Fang, L. Li, and Z. Chen, "Comparison of ring artifacts removal by using neural networks in different domains", Poster presented at the IEEE Nuclear Science Symposium and Medical Imaging Conference, Manchester, UK, 2019.

[13] Z. Chao and H.-J. Kim, "Removal of computed tomography ring artifacts via radial basis function artificial neural networks", *Physics in Medicine and Biology*, vol. 64, no. 23, p. 235 015, Dec. 2019.

[14] O. Ronneberger, P. Fischer, and T. Brox, "U-net: Convolutional networks for biomedical image segmentation", in *International Conference on Medical Image Computing and Computer-Assisted Intervention*, Springer, 2015, pp. 234–241.

[15] H. S. Park, S. M. Lee, H. P. Kim, *et al.*, "CT sinogram-consistency learning for metal-induced beam hardening correction", *Medical Physics*, vol. 45, no. 12, pp. 5376–5384, 2018.

[16] W.-A. Lin, H. Liao, C. Peng, *et al.*, "DuDoNet: Dual Domain Network for CT metal artifact reduction", in *Proceedings of the IEEE Conference on Computer Vision and Pattern Recognition*, 2019, pp. 10 512–10 521.

[17] V. Nair and G. E. Hinton, "Rectified linear units improve restricted boltzmann machines", in *Proceedings of the 27th International Conference on Machine Learning (ICML-10)*, 2010, pp. 807–814.

[18] D. P. Kingma and J. Ba, "Adam: A method for stochastic optimization", *arXiv preprint arXiv:1412.6980*, 2014.

[19] Martin Abadi, Ashish Agarwal, Paul Barham, *et al.*, *TensorFlow: Large-scale machine learning on heterogeneous systems*, Software available from tensorflow.org, 2015.

[20] K. Clark, B. Vendt, K. Smith, *et al.*, "The Cancer Imaging Archive (TCIA): Maintaining and operating a public information repository", *Journal of Digital Imaging*, vol. 26, no. 6, pp. 1045–1057, 2013.

[21] W. van Aarle, W. J. Palenstijn, J. Cant, *et al.*, "Fast and flexible X-ray tomography using the ASTRA toolbox", *Optics Express*, vol. 24, no. 22, pp. 25 129–25 147, 2016.

[22] F. De Carlo, D. Gürsoy, D. J. Ching, *et al.*, "Tomobank: A tomographic data repository for computational X-ray science", *Measurement Science and Technology*, vol. 29, no. 3, p. 034 004, 2018.

[23] D. Gürsoy, F. De Carlo, X. Xiao, *et al.*, "TomoPy: A framework for the analysis of synchrotron tomographic data", *Journal of Synchrotron Radiation*, vol. 21, no. 5, pp. 1188–1193, 2014.

[24] Z. Wang, A. C. Bovik, H. R. Sheikh, *et al.*, "Image quality assessment: From error visibility to structural similarity", *IEEE Transactions on Image Processing*, vol. 13, no. 4, pp. 600–612, 2004.

[25] B. Münch, P. Trtik, F. Marone, *et al.*, "Stripe and ring artifact removal with combined wavelet—Fourier filtering", *Optics Express*, vol. 17, no. 10, pp. 8567–8591, 2009.

[26] E. X. Miqueles, J. Rinkel, F. O'Dowd, *et al.*, "Generalized Titarenko's algorithm for ring artefacts reduction", *Journal of Synchrotron Radiation*, vol. 21, no. 6, pp. 1333–1346, 2014.